LA-UR- 08-7941

Approved for public release;
distribution is unlimited.

Title:	X-ray Line Polarization Spectroscopy of Li-Like Si Satellite Line Spectra
Author(s):	Peter Hakel, Roberto C. Mancini, Joseph Abdallah Jr., Manolo Sherrill, Honglin Zhang.
Intended for:	Journal of Physics B

Los Alamos
NATIONAL LABORATORY
EST. 1943

Form 836 (7/06)

X-ray Line Polarization Spectroscopy of Li-like Si Satellite Line Spectra

P Hakel[1], R C Mancini[1], J Abdallah[2], M E Sherrill[2] and H L Zhang[2]

[1]Department of Physics, University of Nevada, Reno, Nevada 89557, USA
[2]Los Alamos National Laboratory, Los Alamos, New Mexico 87545, USA

Abstract. We apply the magnetic-sublevel atomic kinetics model POLAR to the calculation of polarization properties of satellite lines in Li-like Si driven by subpicosecond-duration laser pulses. We identify spectral lines whose polarization can serve as a marker of plasma anistropy due to anisotropy in the electron distribution function. We also discuss the utility and limitations of our current theoretical approach and point out possible future improvements and directions.

PACS numbers: 52.38.Ph, 32.30.Rj

Keywords: X-rays, polarization, satellite lines, laser plasmas, magnetic sublevels
Submitted to: *J. Phys. B: At. Mol. Phys.*

1. Introduction

Polarization-sensitive measurements of spectral lines can provide an insight into anisotropic qualities of plasmas. For instance, directional electrons generated by the interaction of short and intense laser pulses with a target can create alignment in upper levels of spectral line transitions. Alignment is defined as unequal population of the magnetic sublevels of a given atomic fine structure energy level. The radiative decay of aligned levels is characterized by different intensities of the two polarization-specific components of the spectral line. The relative difference between these two components is the line's polarization degree and signifies the presence of anisotropy in the plasma.

In the past polarization spectroscopy has been employed in a variety of contexts and applications. For example, anistropic plasma characteristics were inferred from polarized line emissions emitted by solar flares [1], laser-produced plasmas (in Fe [2] and in Al [3, 4]), and Z-pinches [5]. Detailed atomic physics studies focused on the mechanisms of polarization formation were carried out both theoretically [6, 7, 8] as well as experimentally [9, 10, 11] for Fe emissions. These studies revealed the value of both the resonance as well as dielectronic satellite lines as possible polarized indicators

of plasma anisotropy. The effects of cascades were addressed, for instance, in [8] and placed into a general non-perturbative multilevel atomic kinetics context in [12, 13]. We have applied a similar technique to the study of polarized Fe line emissions from the EBIT [14] as well as laboratory Si plasmas [15] with the automatic treatment of cascade effects via multilevel kinetics. Recently, the polarization properties of the He-α resonance line in Cl were measured, modeled, and interpreted in terms of an anisotropic electron distribution function [16, 17, 18]. Overviews of state-of-the-art of polarization modeling have been summarized in [19, 20, 21].

In this paper we study how a particular type of plasma anisotropy (a beam of energetic electrons) can reveal itself through the polarization of He-α satellite lines in Li-like Si arising from transitions between autoionizing $1s\ 2l\ 2l'$ with $l, l' = s, p$ upper states and $1s^2\ 2l$ lower states. We identify the best candidates for anisotropy markers and discuss the formation of the polarization effect.

2. Model

The technique employed in this work is the collisionally-radiative magnetic-sublevel atomic kinetics model POLAR. We described the details of this model in a previous publication [15] to which we hereafter refer as Paper I. POLAR calculates the magnetic-sublevel populations based on the time-histories of plasma conditions, in particular, the electron distribution function. The electron pool is modeled having two components: a thermal part whose temperature is calculated by a one-dimensional Lagrangian hydrodynamics code FILM [22] and a non-thermal part computed by a 1 1/2-dimensional particle-in-cell code EUTERPE [23]. The overall ionization balance as a function of time is calculated by another collisional-radiative model M3R [24] and its results serve as input for the detailed sublevel code POLAR. The organization and relationships of this suite of codes are graphically presented in figure 1 of Paper I.

Magnetic-sublevel populations are post-processed into polarization-dependent total line intensities, spectra, and polarization degrees. This is done in the optically-thin approximation which is appropriate for satellite line emissions in laboratory plasmas (see Paper I). (We discuss the potential opacity effects on line polarization in another publication [25].) As in Paper I, we study the polarized satellite line emissions from Si plasmas driven by high-intensity ultrashort-duration laser pulses. We use the results of hydrodynamics (FILM), electron-kinetics (EUTERPE), and ionization-balance (M3R) calculations presented in Paper I. These models provide the plasma conditions required to drive the detailed calculation of magnetic sublevel populations performed by POLAR. In this work, however, we turn our attention from He-like Si to another ion stage of Si and investigate the polarization characteristics of the n=2 satellites to the He-α resonance line. These spectral lines are defined by the $1s\ 2l\ 2l' \rightarrow 1s^2\ 2l$ group of transitions in the Li-like ion. To this end we constructed a magnetic-sublevel model for the purposes of the POLAR calculation consisting of configurations $1s^2\ 2l$, $1s^2\ 3l$, and $1s\ 2l\ 2l'$ (see figure 1). The $1s^2\ 3l$ complex is included in the model to provide a more

complete account of multilevel (a.k.a. cascade) effects in the atomic kinetics. Total line intensities provided by POLAR are spread out into synthetic spectra using the Voigt lineshapes which are appropriate for the relatively low densities (less than 10^{22} cm^{-3}) achieved during the line emission (see figure 3 in Paper I).

The populations of magnetic sublevels depicted in figure 1 are determined by the competition between the rates of atomic processes linking individual sublevels to one another. In this model we account for electron collisional excitation, collisional deexcitation, and spontaneous radiative decay that connect states within the Li-like ion. We also add autoionization and electron capture, which are processes linking the $1s\ 2l\ 2l'$ states to the ground state of the He-like ion. In [15] we also considered elastic scattering of electrons that can redistribute populations among the magnetic sublevels of the same fine-structure J-level (see figure 7 in Paper I). This is a process that does not need to be included in the traditional (i.e., J-level, LS-term, configuration-average, etc.) atomic kinetics because it has no bearing on the energy-level population at the relevant detail of description of the energy-level structure. In Paper I we found that elastic scattering did not have a significant effect at the plasma conditions considered in this work, and therefore we omitted this process from the model in the present work.

The atomic structure and collision data were calculated with the Los Alamos suite of codes CATS [26, 27], ACE [28], and GIPPER [29]. CATS provides the energy-level structure (see figure 1) and J-level spontaneous radiative decay rates (115 electric dipole transitions). Spontaneous radiative decay rates between magnetic-sublevel are calculated from the J-level rates via the Wigner-Eckart theorem (see, for example, equation 4 in [14]). ACE was used to construct a database of 520 magnetic-sublevel electron-impact excitation cross sections covering all possible transitions, with the exception of the connections between $1s^2\ 3l$ and $1s\ 2l\ 2l'$ levels. (These transitions require the "relocation" of two electrons and are therefore weak.) 15 J-level autoionization rates between $1s\ 2l\ 2l'$ and $1s^2$ were calculated by GIPPER; magnetic-sublevel rates of electron capture were formed from these autoionization rates using the technique described in the Appendix of [14].

The collection of transitions that are candidates for polarization markers in the spectra is given in table 1. We note that there are two distinct levels characterized by $1s\ 2s\ 2p\ ^2P_{3/2}$. These two levels differ in their intermediate angular momentum coupling arrangement. Here we distinguish them with an additional label that assigns (1) to the state of the lower energy and (2) to the more energetic state. Our model also includes two J-levels characterized as $1s\ 2s\ 2p\ ^2P_{1/2}$, which we also distinguish by additional (1) and (2) labels assigned according to the energy. Lines associated with these latter two levels do not appear in table 1 because, like all lines originating from $J = 1/2$ levels, they are always unpolarized under axially symmetric conditions ($f_M = f_{-M}$, where f represents the sublevel populations).

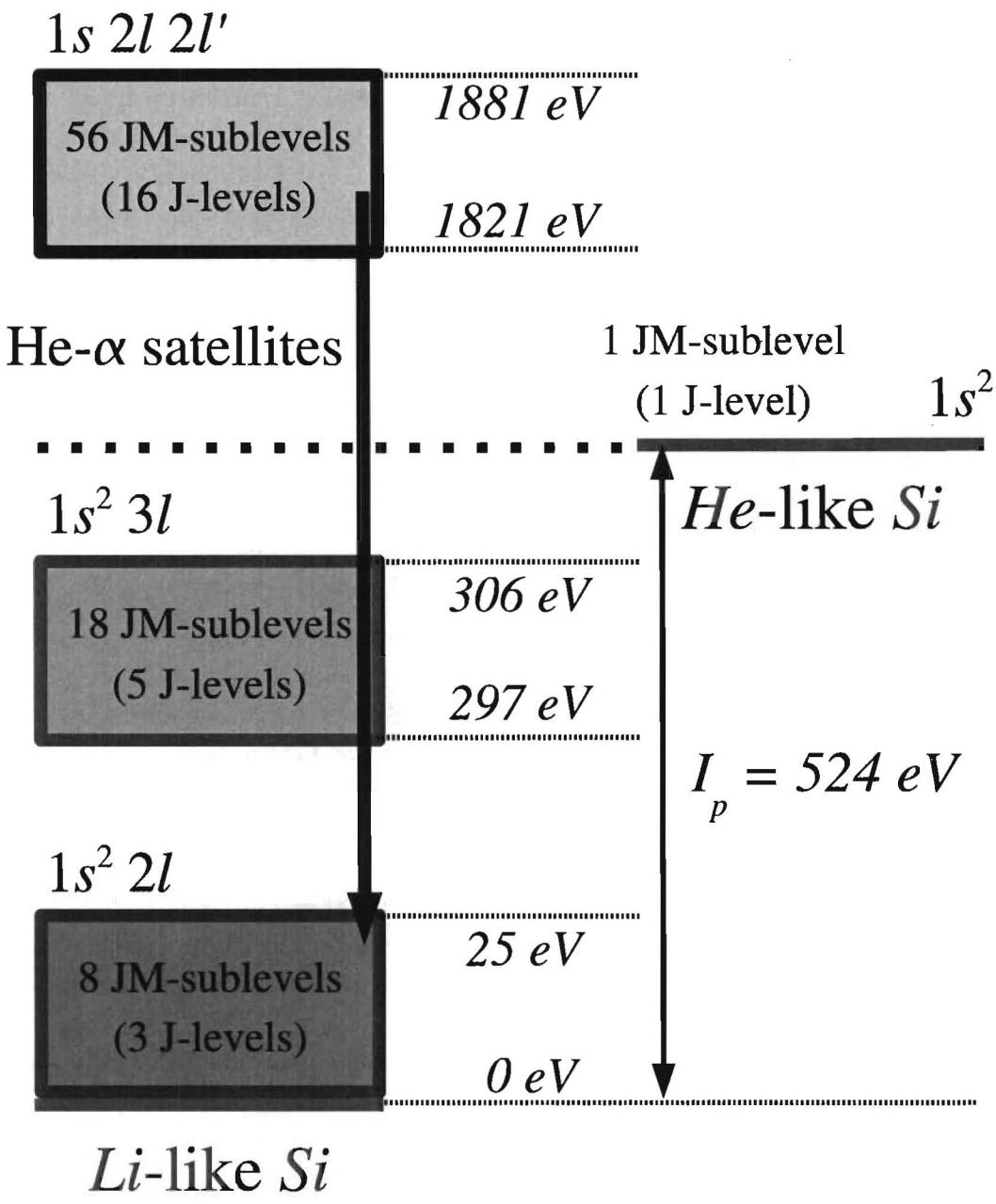

Figure 1. Schematic illustration of the energy level structure included in POLAR for studying the polarization properties of the n=2 Li-like satellites to the He-α Si line.

Table 1. He-α satellite transitions in Si between 1840 and 1860 eV.

Label	Line transition	Photon energy (eV)
1	$1s\ 2s\ 2p\ (2)\ ^2P_{3/2} \rightarrow 1s^2\ 2s\ ^2S_{1/2}$	1855
2	$1s\ 2s\ 2p\ (1)\ ^2P_{3/2} \rightarrow 1s^2\ 2s\ ^2S_{1/2}$	1846
3	$1s\ 2p^2\ ^2P_{3/2} \rightarrow 1s^2\ 2p\ ^2P_{3/2}$	1844
4	$1s\ 2p^2\ ^2D_{3/2} \rightarrow 1s^2\ 2p\ ^2P_{1/2}$	1841
5	$1s\ 2p^2\ ^2P_{5/2} \rightarrow 1s^2\ 2p\ ^2P_{3/2}$	1840

3. Results

In Figs. 2 - 5 we present the time and space-integrated polarization-dependent spectra consisting of satellite lines to the Si He-α line. The spatial integration extends over the "skin-depth" region of the target (see figure 2 in Paper I). It was in this region of the target where the plasma conditions led to noticeable polarization effects in He-like satellites of the Ly-α (Paper I) which is why we study this region in the present work as well. The FILM code used to model the hydrodynamic behavior of the target is a one-dimensional Lagrangian hydrodynamics code whose fluid elements (a.k.a. cells) can therefore be labeled by their relative initial positions in the target before the laser strikes. In our model cells # 1 through 50 are located in the "bulk" and "conduction" regions of the Si target. The region of our interest is 0.05 microns thick and is partitioned into 76 cells of progressively decreasing thickness with labels 51 through 126. Cells placed closer to the target surface tend to experience higher temperatures and lower densities as the time goes forward than their more deeply located counterparts (figure 3 in Paper I).

The time integration covers the time interval of approximately 1 ps during and after the 300 fs long laser pulse peaking at 400 fs. The figures represent the results computed for four different laser intensities: 2×10^{16}, 5×10^{16}, 1×10^{17}, and 5×10^{17} W/cm^2. The hot electron fraction α (which is a free parameter in our model) is set to 0.2 in accordance with previous estimates for this range of laser intensities [30].

In all four cases we observe that the two strongest lines both show noticeable polarization effect. These are the lines # 2 ($1s\ 2s\ 2p\ (1)\ ^2P_{3/2} \rightarrow 1s^2\ 2s\ ^2S_{1/2}$) and # 3 ($1s\ 2p^2\ ^2P_{3/2} \rightarrow 1s^2\ 2p\ ^2P_{3/2}$), according to the labeling from table 1. Therefore they emerge as the primary polarization markers of plasma anisotropy from among the studied satellite lines to the Si He-α. If we use the standard definition of the polarization degree $P \equiv (I_{||} - I_{\perp})/(I_{||} + I_{\perp})$ with the peak line intensities, we obtain values $P = 0.08$ for line 3 and $P = 0.17$ for line 2. In figure 6, figure 7, and figure 8 we show how the polarization degrees of the two lines evolve as a function of time. Each figure displays results for a different fluid element in the "skin depth" region of the target (see figure 2 in Paper I). A comparison of these three figures reveals the presence of spatial gradients in the formation of the polarized line emissions. A non-trivial time

development of the polarization degrees is also apparent from these figures. For instance, in figure 7 we observe that while the polarization of line 2 does not change much as the time progresses, line 3 shows a significant development. Its gradual transition from negative to positive values of P leads to a smaller polarization result than in line 2 in the time-integrated spectrum of figure 3. This illustrates the importance of performing fully time-dependent kinetics modeling in cases of transient laboratory plasmas. Spatial gradients are addressed by separate modeling of the various plasma regions.

We used the feeding-channel diagnostic tool of POLAR to rank the atomic processes according to their importance in populating the upper levels of the two transitions of interest. This diagnostic combined with the time-dependent nature of our model allows us to identify the population-kinetic mechanisms responsible for the polarized line formation and their evolution with time and plasma conditions. For the purpose of illustration we focused on the fluid element # 90 as a representative of the "skin-depth" region of the plasma. The upper level of line 2 ($1s\ 2s\ 2p\ (1)\ ^2P_{3/2}$) is primarily populated via collisional excitation from the ground state ($1s^2\ 2s\ ^2S_{1/2}$) throughout the time span of the simulation. The electron capture process from the ground state of the He-like ion starts as the second most-important feeding channel but its importance wanes as the time goes on. Electron capture is gradually replaced by the collisional excitation from $1s^2\ 2p\ ^2P_{3/2}$ as the second most important influx of population. In any case, however, the collisional excitation from the ground state to the upper level of line 2 remains roughly one order of magnitude stronger than the second most-important feeding channel, whichever it is at a given time. We therefore conclude that the polarization degree of line 2 is primarily determined by the anisotropic collisional excitation of $1s\ 2s\ 2p\ (1)\ ^2P_{3/2}$ from the ground state of the Li-like ion.

The feeding channel diagnostic of line 3 shows a slightly different scenario. At the beginning of the simulation the most important feeding channel is the electron capture from $1s^2$. This process beats the runner up (collisional excitation from $1s^2\ 2p\ ^2P_{3/2}$) by about an order of magnitude. However, the autoionization rate of $1s\ 2s\ 2p\ (1)\ ^2P_{3/2}$ is in fact 1.55 times larger than that of $1s\ 2p^2\ ^2P_{3/2}$, so this difference in behavior cannot be attributed to electron capture. It is in fact, the relative weakness of the collisional excitation into $1s\ 2p^2\ ^2P_{3/2}$ that allows the electron capture process to dominate early in time. The collisional connection of this level with the Li-like ground state is weak since it requires that not one but two electrons change subshells. This, combined with the observation that the excited states get noticeably less population than the ground states, leads to the dominance of electron capture into $1s\ 2p^2\ ^2P_{3/2}$ early in time. Further on, however, the changes in plasma conditions gradually add population to the excited states and eliminate the electron capture process from contention in the kinetics. These observations can explain the qualitatively different time dependences of the two polarization degrees of the two lines for the fluid element # 90 (figure 7). Line 2 is dominated by the same feeding channel throughout the simulation history and its polarization therefore does not change very much. Line 3, on the other hand, is controlled at different times by two different processes that each push the level alignment

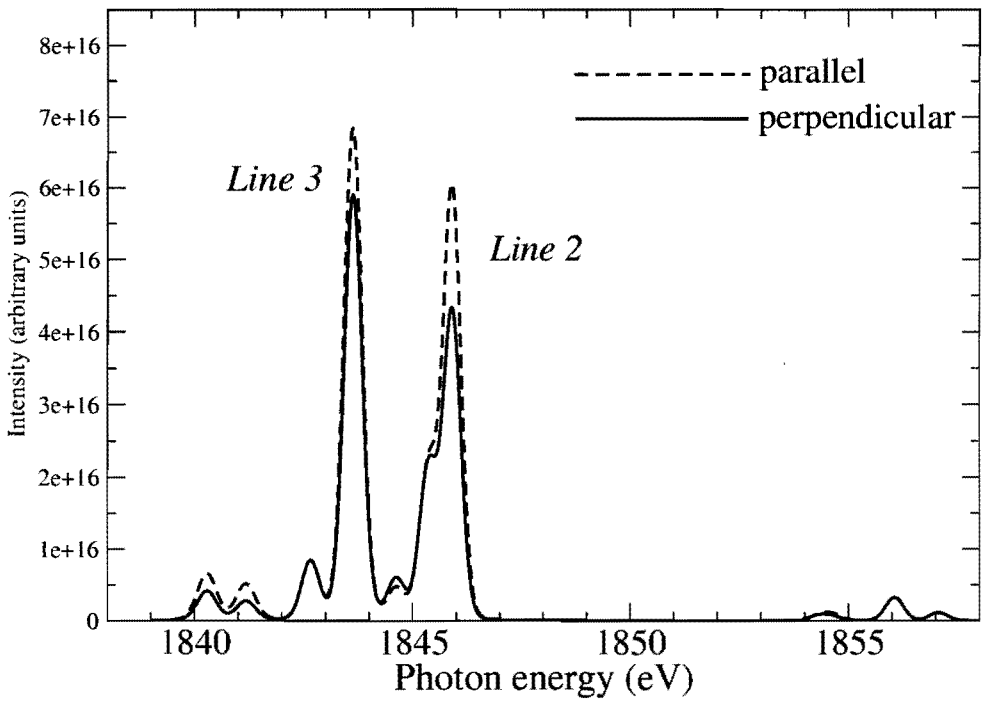

user

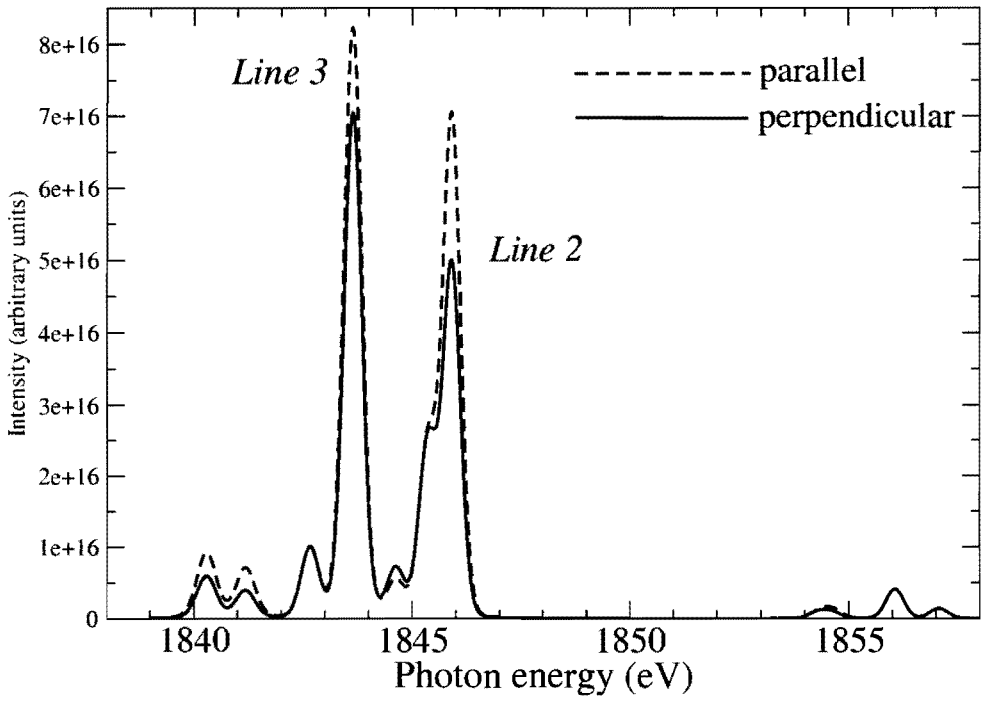

Figure 3. Time and space-integrated polarization-dependent spectra for laser intensity $I = 5 \times 10^{16}\ W/cm^2$ and $\alpha = 0.2$.

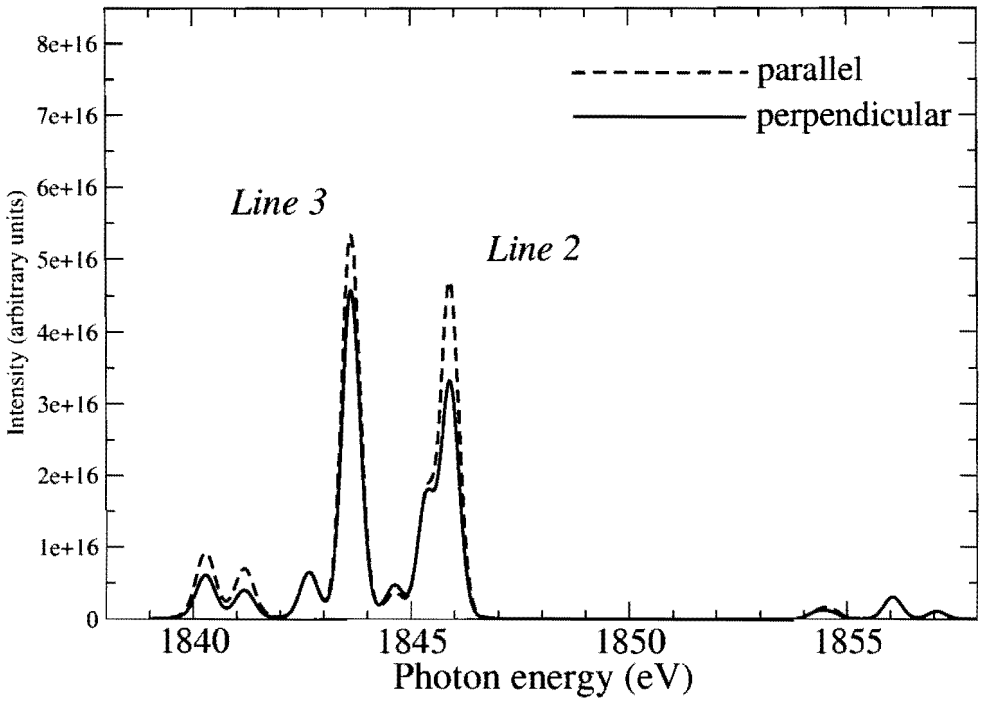

ıser

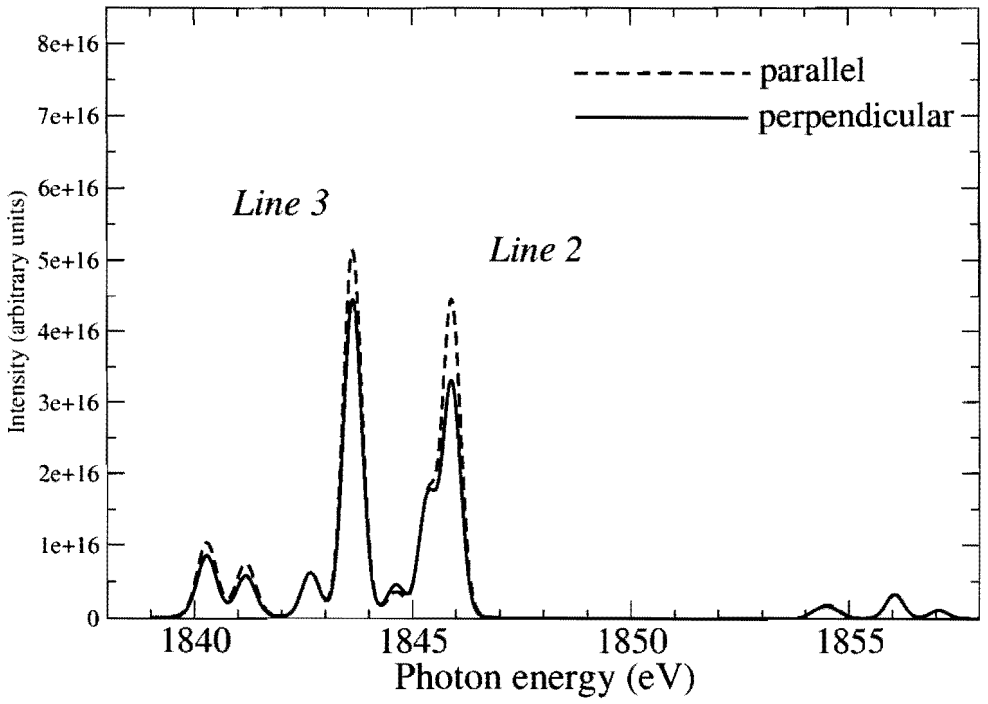

Figure 5. Time and space-integrated polarization-dependent spectra for laser intensity $I = 5 \times 10^{17}\ W/cm^2$ and $\alpha = 0.2$.

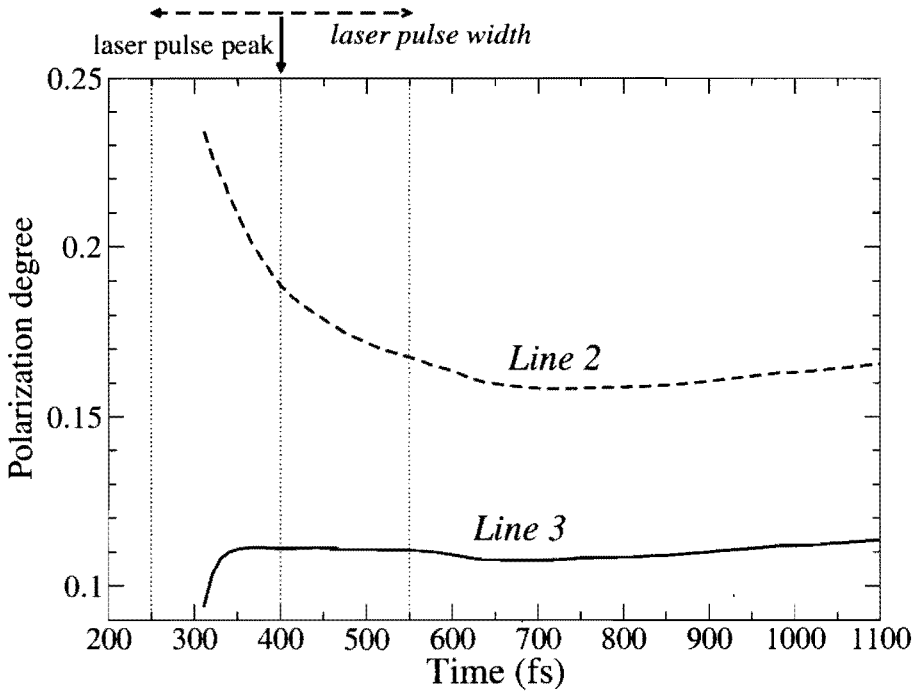

Figure 6. Time and space-resolved polarization degrees for laser intensity $I = 5 \times 10^{16}$ W/cm^2 and $\alpha = 0.2$ for fluid element # 60.

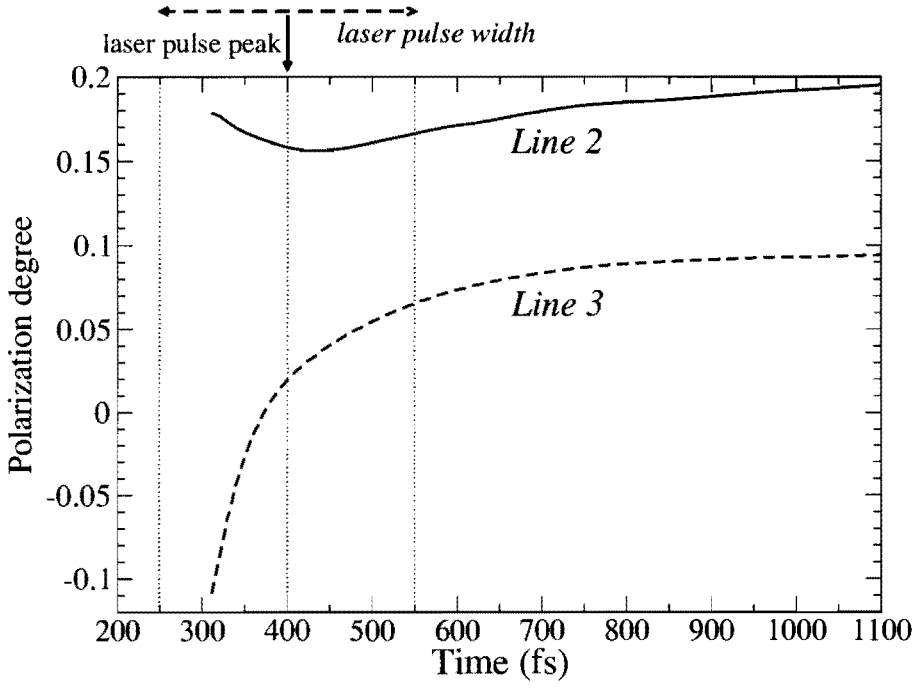

Figure 7. Time and space-resolved polarization degrees for laser intensity $I = 5 \times 10^{16}$ W/cm^2 and $\alpha = 0.2$ for fluid element # 90.

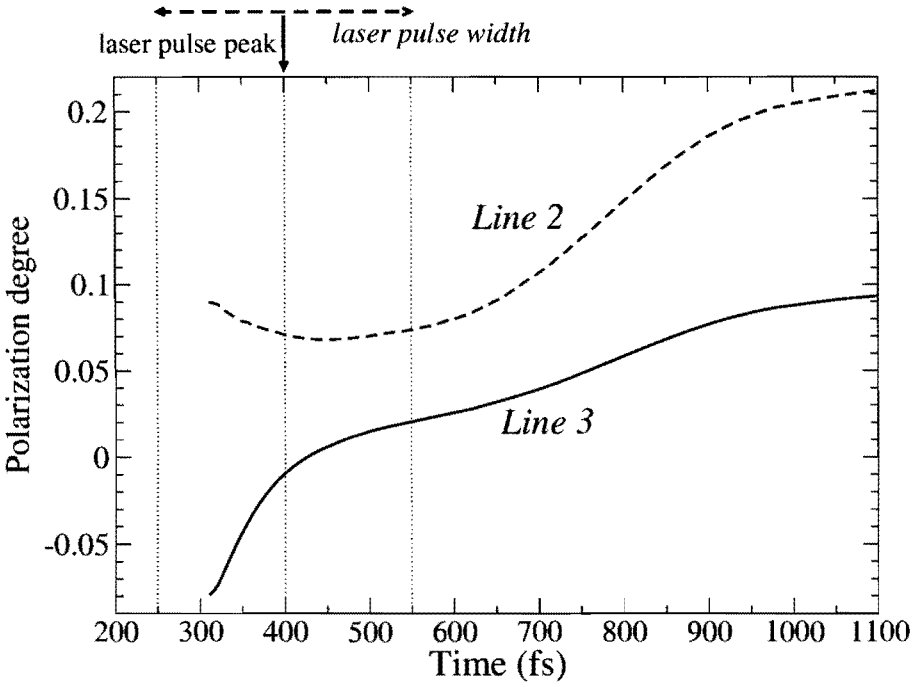

Figure 8. Time and space-resolved polarization degrees for laser intensity $I = 5 \times 10^{16}$ W/cm^2 and $\alpha = 0.2$ for fluid element # 120.

(and hence line polarization) in opposite directions. Polarization of line 3 therefore starts negative and ends positive, yielding a smaller time-integrated value than line 2.

We also observe that time-integrated polarization values of the lines are essentially independent of the laser intensity. This differs from the findings of Paper I (see table IV) where the polarization degree of a marker line decreased with increasing laser intensity, while the hot electron fraction α was held constant. Strictly speaking, the hot electron fraction is not independent of laser intensity and therefore treating it as an additional free parameter is not quite rigorous. This complication was partially addressed in Paper I where we calculated polarization degrees for various laser intensities *and* hot electron fractions (see table IV and figure 11 in Paper I). A more satisfactory model would characterize the electron distribution in its entirety (i.e., both its thermal and non-thermal parts) by a single electron-kinetics simulation for given laser pulse characteristics. Improvement of POLAR along these lines is currently under consideration for future development.

We also point out the partial blending of another relatively strong line into the low-energy wing of line 2. This illustrates how the diagnostic value of a chosen spectral line can be affected by its overlap with another line. Spectral lines overlap and blend when their widths are comparable with their energy separation. This can occur if either of two following conditions are met: 1) the lines are intrinsically closely spaced due to the rich energy level structure (as is typical in many-electron atoms), or, 2) lines are sufficiently widened by Stark broadening in high-density plasma environment. In such

cases, detailed multilevel and mutliline theoretical modeling such as POLAR is needed to properly interpret experimental spectra that may be deceptively lacking of rich line structure.

4. Conclusions

We carried out model calculations of the time-dependent magnetic-sublevel atomic kinetics and polarization-dependent Li-like Si X-ray satellite lines driven by subpicosecond-duration laser pulses taking into account hydrodynamics, electron kinetics, and collisional-radiative atomic kinetics. Transient effects and spatial gradients were addressed as well. Two dominant and polarized satellites to the Si He-α ($1s\ 2s\ 2p\ (1)\ ^2P_{3/2} \rightarrow 1s^2\ 2s\ ^2S_{1/2}$) and ($1s\ 2p^2\ ^2P_{3/2} \rightarrow 1s^2\ 2p\ ^2P_{3/2}$) were identified as possible markers of plasma anisotropy. The calculations were performed in the optically thin approximation. The electron distribution function was modeled as combination of a thermal (Maxwellian) and a non-thermal ("beam") component. Future work is planned to further enhance the model by considering a unified description of the electron distribution which will improve its internal consistency. Future extension of this model should also include the treatment of opacity effects on intensities and polarization degrees of spectral lines.

Acknowledgments

This work was supported by the NSHE and by Los Alamos National Laboratory, operated by Los Alamos National Security LLC under contract DE-AC52-06NA25396 from the U.S. Department of Energy (NNSA).

References

[1] Shlyaptseva A S, Urnov A M and Vinogradov A V *P. N. Lebedev Phys. Inst. Report* No. 194 (unpublished)
[2] Inal M K and Dubau J 1987 *J. Phys. B* **20** (16) 4221
[3] Kieffer J C, Matte J P, Pépin H, Chaker M, Beaudoin Y, Johnston T W, Chien C Y, Coe S, Mourou G and Dubau J 1992 *Phys. Rev. Lett.* **68** 480
[4] J. C. Kieffer, J. P. Matte, M. Chaker, Y. Beaudoin, C. Y. Chien, S. Coe, G. Mourou, J. Dubau, and M. K. Inal, *Phys. Rev. E* **48**, 4648 (1993) Kieffer J C, Matte J P, Chaker M, Beaudoin Y, Chien C Y, Coe S, Mourou G, Dubau J and Inal M K 1993 *Phys. Rev. E* **48** 4648
[5] Walden F, Kunze H J, Petroyan A, Urnov A and Dubau J 1999 *Phys. Rev. E* **59** 3562
[6] Inal M K and Dubau J 1989 *J. Phys. B* **22** (20) 3329
[7] Csanak G, Cartwright D C and Trajmar S 1992 *Phys. Rev. A* **45** 1625
[8] Inal M K and Dubau J 1993 *Phys. Rev. A* **47** 4794
[9] Beiersdorfer P, Vogel D A, Reed K J, Decaux V, Scofield J H, Widmann K, Hölzer G, Förster E, Wehrham O, Savin D W and Schweikhard L 1996 *Phys. Rev. A* **53** 3974
[10] Shlyaptseva A S, Mancini R C, Neill P, Beiersdorfer P, Crespo López-Urrutia J R and Widmann K 1998 *Phys. Rev. A* **57** 888
[11] Shlyaptseva A S, Mancini R C, Neill P, Beiersdorfer P 1999 *J. Phys. B* **32** 1041
[12] Omont A 1977, *Prog. Quantum Electron.* **5** 69

[13] Fujimoto T and Kazantsev S 1997 *Plasma Phys. Controlled Fusion* **39** 1267
[14] Hakel P, Mancini R C, Harris C, Neill P, Beiersdorfer P, Csanak G and Zhang H L 2007 *Phys. Rev. A* **76** 012716
[15] Hakel P, Mancini R C, Gauthier J C, Mínguez E, Dubau J and Cornille M 2004, *Phys. Rev. E* **69** 056405
[16] Kai T, Nakazaki S, Kawamura T, Nishimura H and Mima K 2007 *Phys. Rev. A* **75** 012703
[17] Inubushi Y, Kai T, Nakamura T, Fujioka S, Nishimura H and Mima K 2007 *Phys. Rev. E* **75** 026401
[18] Kawamura T, Kai T, Koike F, Nakazaki S, Inubushi Y and Nishimura H 2007 *Phys. Rev. Lett.* **99** 115003
[19] del Toro Iniesta J C 2003 *Introduction to Spectropolarimetry* (Cambridge University Press)
[20] Landi Degl'Innocenti E and Landolfi M 2004 *Polarization in Spectral Lines* (Kluwer Academic Publishers)
[21] T. Fujimoto and A. Iwamae (Editors) 2008 *Plasma Polarization Spectroscopy* (Springer-Verlag)
[22] Teubner U, Gibbon P, Förster E, Falliès F, Audebert P, Geindre J P and Gauthier J C 1996 *Phys. Plasmas* **3** 2679
[23] Bonnaud G and Reisse G 1986 *Nucl. Fusion* **26** 633; Lefebvre E 1996 Ph.D. thesis, Université de Paris XI, Orsay
[24] Mancini R C and Mínguez E 1996, First International NLTE Atomic Kinetics Workshop, Gaithersburg, MD (unpublished); Lee R W, Nash J K and Ralchenko Y 1997, *J. Quant. Spectrosc. Radiat. Transf.* **58** 737
[25] Hakel P and Mancini R C, submitted to *Astronomy and Space Science* (Proceedings of the April 2008 APS HEDLA meeting, St. Louis, MO)
[26] Cowan R D 1981 *The Theory of Atomic Structure and Spectra* (University of California Press, Berkeley)
[27] Abdallah J, Clark R E H and Cowan R D 1988 Los Alamos National Laboratory Report No. LA-11436-M, Vol. I (unpublished)
[28] Clark R E H, Abdallah J, Csanak G, Mann J B and Cowan R D 1988, Los Alamos National Laboratory Report No. LA-11436-M, Vol. II (unpublished)
[29] Archer B J, Clark R E H, Fontes C J and Zhang H L 2002 Los Alamos National Laboratory Report No. LA-02-1526 (unpublished)
[30] Rousse A, Audebert P, Geindre J P, Falliès F, Gauthier J C, Mysyrowicz A, Grillon G and Antonetti A 1994 *Phys. Rev. E* **50** 2200